ChemComm

COMMUNICATION

View Article Online
View Journal | View Issue

Cite this: *Chem. Commun.*, 2023, 59, 5059

Received 8th December 2022,
Accepted 23rd March 2023

DOI: 10.1039/d2cc06696c

rsc.li/chemcomm

Peptide photowrapping of gold-silica nanocomposites for constructing MMP-responsive drug capsules for chemo-photothermal therapy†

Hao Liu,‡[a] Sijie He,‡[a] Li-Ya Niu,[b] Xue-Wang Gao,[c] Ke Feng,[c] Shumin Yang,[a] Jianqun Shao,[a] Wenhua Zhao,[a] Nan Xie *[a] and Qing-Zheng Yang[b]

A multifunctional undecapeptide, YYDPLGLADYY, was designed and synthesized for the photowrapping of silica-coated gold nanorods. The obtained nanocapsules, bearing a well-defined core–shell structure, were able to encapsulate a therapeutic drug, respond to an MMP-upregulated tumor microenvironment, and achieve NIR-triggered anticancer chemo-photothermal therapy with favorable efficacy.

Tumor microenvironment (TME) response is recognized as one of the important design strategies for therapeutic nanocarriers,[1,2] where a drug delivery system (DDS) passively responds to environmental changes such as a decrease in pH, hypoxia conditions, and altered expression of certain enzymes.[3,4] Regarding the enzymes, matrix metalloproteinases (MMPs) have been observed to be an overexpressed biomarker in most malignant tumors.[5,6] Due to the excessive enzymatic activity response, an upregulated MMP would facilitate automatic tailoring to substrates and lead to ligand activation, electrostatic conversion, or protective layer deshielding, thus realizing specific targeting and on-demand payload release at tumor sites.[7,8] Through molecular assembly or covalent association, diverse composites have been established based on peptides,[9–12] proteins,[13] polymers,[14–16] and inorganic hybrids,[17,18] but controlling the timing and precise release of cargo by MMP-mediated nanocarriers is still thwarted by the occurrence of passive responses.[19,20]

The silica-coated gold nanorod (Au@SiO_2) is a prime example of a suitable platform for both photothermal therapeutics and drug delivery owing to its unique combination of a plasmonic gold core and mesoporous silica shell structure.[21–23] With its exceptional feature of localized surface plasmon resonance (LSPR), the inner gold metal nanorod shows tunable responsiveness to light irradiation and provides a target manipulation pathway for photothermal therapy.[24] Bearing a high mesoporous volume, the outer silica shell has a large encapsulation capacity, *i.e.*, to load guest cargos; moreover, its reactive Si-OH surface can be covalently modified in various ways and hence allows for additional functionalities to be produced for various theranostic scenarios.[25–28]

Most recently, an *in situ* grafting-cleavage strategy was developed to incorporate programmable peptide sequences onto silica surfaces, by which photoactive residues could be facilely introduced to fabricate nanohybrids.[29] On this basis, we designed in the current work an amphiphilic undecapeptide (YYDPLGLADYY) for the construction of photochemically MMP-responsive Au@SiO_2 nanocapsules (Scheme 1). Structurally, the peptide sequence was designed to contain three functional segments: (1) a specific PLGLA segment to react to MMP upregulation and enzymic cleavage for a smart response in TME; (2) dityrosine (YY) segments at both ends of the peptide to serve as crosslinkers and hence photowrap drug-loaded silica and gate mesoporous orifices for on-demand release; (3) aspartic acid (D) residues to regulate charge distribution and optimize blood circulation. Utilizing modifiable Au@SiO_2 as a functional platform, we set out to construct a smart and photomanipulable drug delivery system for chemo-photothermal therapy.

The peptide-shelled gold-silica nanocapsules were designed as shown in Scheme 1. Au@SiO_2 was prepared according to the reported method[29] and was employed as a multifunctional platform for photothermal therapeutics and drug delivery. For the purpose of NIR photothermal therapy, the wavelength of the major LSPR peak of the Au metal core was tuned to ~800 nm by adjusting the aspect ratio to 4.2 ± 0.9, and then the Au core was coated with mesoporous silica having a controlled thickness of ~21 nm (Fig. S1, ESI†). The MMP-responsive undecapeptide YYDPLGLADYY was synthesized using standard *N*-(9-fluorenyl) methoxycarbonyl (Fmoc) solid-phase peptide synthesis (SPPS), and identified using high-resolution mass spectrometry (HRMS) and nuclear magnetic resonance (^{1}H NMR)

[a] *School of Pharmaceutical Sciences, Capital Medical University, Beijing 100069, P. R. China. E-mail: nanxie@ccmu.edu.cn*
[b] *Key Laboratory of Radiopharmaceuticals Ministry of Education, College of Chemistry, Beijing Normal University, Beijing 100875, P. R. China*
[c] *Key Laboratory of Photochemical Conversion and Optoelectronic Materials, Technical Institute of Physics and Chemistry, the Chinese Academy of Sciences, Beijing 100190, P. R. China*

† Electronic supplementary information (ESI) available. See DOI: https://doi.org/10.1039/d2cc06696c

‡ Equal contribution.

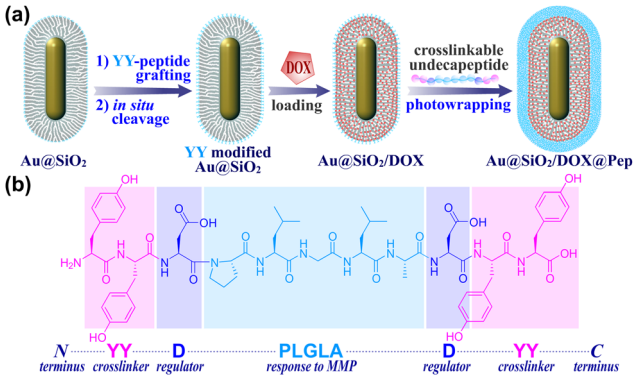

Scheme 1 (a) The fabrication of peptide-photowrapped Au@SiO_2/DOX@Pep nanocapsules, and (b) the design of crosslinkable undecapeptide.

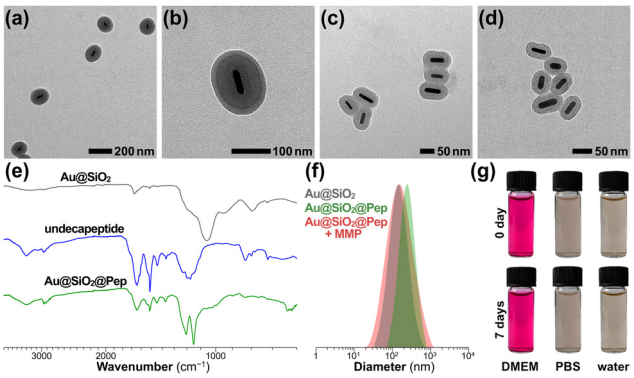

Fig. 1 (a–d) TEM images of Au@SiO_2@Pep (a and b) before and (c) 12 h and (d) 24 h after being incubated with MMP protease. (e) FT-IR spectra of YY-modified Au@SiO_2, undecapeptide YYDPLGLADYY, and Au@SiO_2@Pep. (f) Results of DLS of Au@SiO_2@Pep before and after being incubated with MMP, compared with the results for Au@SiO_2. (g) Photographs of Au@SiO_2@Pep dispersions stored in DMEM, PBS, and water for 0 and 7 days.

spectroscopy (Fig. S16–S19, ESI†). Prior to carrying out the photowrapping, the Au@SiO_2 surface was modified with photoactive YY motifs using an *in situ* grafting-cleavage strategy.[29] Exposure of this modified surface to 405 nm-wavelength (visible-light) irradiation yielded a rapid photocrosslinking of dityrosines on a bilateral undecapeptide with the Au@SiO_2 surface and formed a peptide-shelled structure to afford Au@SiO_2@Pep nanocapsules.[30] Transmission electron microscope (TEM) images of this product showed a well-defined core–shell structure with a diameter of 153 ± 32 nm (Fig. 1a and b). The highly hydrophilic peptide-photowrapped nanocapsules could be well dispersed in an aqueous medium with a surface potential ζ of −35.4 mV (Table S1, ESI†). The dispersions were stable for more than 7 days when stored in a physiological solution such as that containing DMEM or PBS (Fig. 1g). The peptide shell of Au@SiO_2@Pep was confirmed using Fourier transform infrared (FT-IR) spectroscopy (Fig. 1e and Fig. S5, ESI†). As compared to that of Au@SiO_2, the greatly increased absorbance of Au@SiO_2@Pep at 1645, 1516 and 1150 cm^{-1} could be attributed to the effects on the C═O (amide I), N–H (amide II), and phenol-OH characteristic stretchings, respectively, and provided strong evidence for the peptide photocrosslinking through the YY motifs.

To simulate the enzymic response of the peptide shell to upregulated MMP in a tumor microenvironment, MMP protease (collagenase IV) was added to a sample of the Au@SiO_2@Pep dispersion and incubated at 37 °C.[31] Inspection of TEM images of Au@SiO_2@Pep incubated with MMP provided evidence for much of the photowrapped peptide having been stripped off from the gold-silica surface within 12 h of incubation (Fig. 1c)—and nearly all of it stripped off after an additional 12 h of incubation, leaving an exposed bare Au@SiO_2 nanostructure (Fig. 1d). With this shedding, the particle diameter of Au@SiO_2@Pep sharply decreased to 112 ± 18 nm, and corresponding surface potential decreased to −17.9 mV. DLS results also verified these changes in particle diameter, here from 209 ± 41 nm (PDI 0.183) to 143 ± 28 nm (PDI 0.168) (Fig. 1f).

The photothermal performance of gold-silica nanocomposites was assessed by carrying out infrared thermal imaging using an NIR laser. As shown in Fig. 2a and b, the Au@SiO_2@Pep dispersion showed a dramatic increase in temperature that reached a plateau within 12 minutes when subjected to irradiation with 808 nm-wavelength light at 1.0 W cm^{-2}. The rate of temperature increase and the equilibrium temperature reached were proportional to sample concentration. The photothermal stability was tested in four consecutive cycles (Fig. S6, ESI†); good repeatability with almost negligible difference in results was observed from each cycle to the next.

For carrying out a chemo-photothermal combination treatment, DOX was preloaded into Au@SiO_2, which was then photowrapped with the crosslinkable undecapeptide. The obtained Au@SiO_2/DOX@Pep nanocapsules retained the core–shell structure as well as did the empty Au@SiO_2@Pep carrier (Fig. S2, ESI†). The DOX loading content was calculated, based on absorbance of light at 480 nm (Fig. 2c), to be up to 10.8 wt%. In *in vitro* experiments, the MMP-responsive release of DOX from Au@SiO_2/DOX@Pep nanocapsules using Tris–HCl buffer (pH 6) at 37 °C was investigated. As activated collagenase IV was added, 35% of the DOX was released within 12 h of incubation. An obviously hysteretic process was observed. Only 8% of the DOX was found to have been released in the initial 6 h. And then the rate of release quickly accelerated, corresponding to an outburst of loaded DOX into the silica mesopores after the shedding of the peptide. Within a period of 36 h, a 40% cumulative drug release resulted from this MMP-triggered peptide cleavage. Introduction of a photothermal stimulus into the system concurrently with the introduction of the MMP was also tested. Three such photomanipulations, with intermittent NIR irradiation, further boosted the drug release rate to 60%, which was reasonably attributed to a heat-induced diminishment of the electrostatic interactions between loaded DOX and silica mesopores. A comparison of this experiment with a control experiment in the absence of MMP showed that the drug release cannot be provoked merely by NIR irradiation. The results taken together showed peptide photowrapping of the Au@SiO_2 carrier to be a useful method for encapsulating a drug, and for allowing an NIR stimulus to provide a remote photomanipulation for a combined chemo-photothermal treatment.

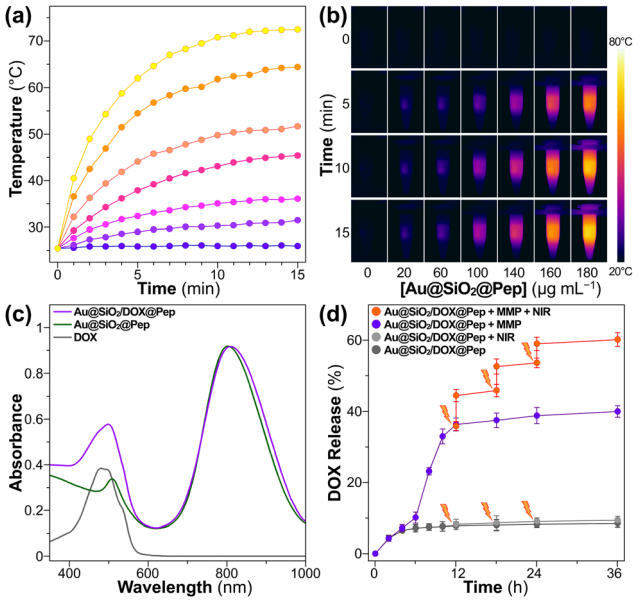

Fig. 2 (a and b) Temperature *versus* time curves and infrared thermographic images of Au@SiO_2@Pep samples of different concentrations upon being exposed to NIR irradiation. (c) UV-Vis spectra of DOX, Au@SiO_2/DOX, and Au@SiO_2/DOX@Pep. (d) DOX release profiles of Au@SiO_2/DOX@Pep at pH 6 upon being exposed to MMP and NIR stimuli.

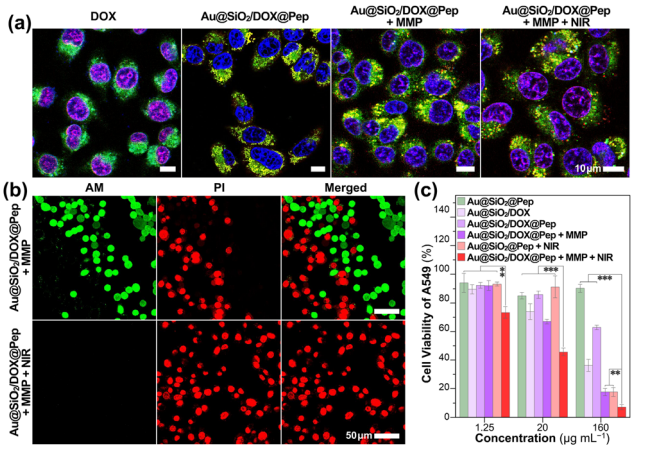

Fig. 3 (a) Merged CLSM images for A549 cells incubated with free DOX and Au@SiO_2/DOX@Pep upon being subjected to MMP and NIR stimuli. (b) Live/dead staining of A549 cells incubated with Au@SiO_2/DOX@Pep upon being subjected to MMP and MMP/NIR stimuli. (c) Viability levels of various samples of A549 cells subjected to different treatments (n = 3). $^{**}p < 0.01$; $^{***}p < 0.001$.

The cellular uptake and intracellular transport of Au@SiO_2/DOX@Pep nanocapsules in A549 cells were investigated using a confocal laser scanning microscope (CLSM, Fig. 3a, Fig. S7, ESI†). In contrast to the accumulation of free DOX in the nucleus through DNA intercalation, DOX loaded in a gold-silica carrier showed subcellular localization, specifically in lysosomes (overlap with LysoTracker Green, Pearson's r = 0.69 ± 0.10), attributed to the photowrapping provided by the peptide shell. As activated collagenase IV was added into system, Au@SiO_2/DOX@Pep nanocapsules responded to the MMP protease and released free DOX, illuminating the lysosomal regions as well as the cell nuclei. After further stimulus with NIR irradiation, more DOX was released, thus promoting the red fluorescence in the nuclei.

The cytotoxicity of Au@SiO_2 nanocomposites was systematically assessed using a standard protocol, namely the MTT assay. Cells remained viable at levels above 85% after being incubated for 24 h and even 48 h with Au@SiO_2@Pep carrier at various concentrations (1.25–160 μg mL^{-1}, Fig. S8, ESI†). The gold-silica nanocapsules exhibited excellent biocompatibility with either tumor or normal cells. And even after DOX was loaded, the resulting Au@SiO_2/DOX@Pep nanocapsules presented just a weak cell-killing effect, showing the peptide photowrapping to be a highly effective shielding method for drug encapsulation (Fig. 3c and Fig. S9, ESI†). As activated collagenase IV was added, significant cytotoxicity was observed for both of A549 and HepG2 cells, which could be attributed to the enzymic-responsive release of DOX in the MMP-upregulated environment. Introduction of an NIR irradiation stimulus appeared to have synergistically promoted drug release,[32,33] specifically the introduction of 808 nm-wavelength laser light greatly slashed the cell viability to as low as 7%. In the meantime, live/dead cell staining assay gave a more visualizable result (Fig. 3b and Fig. S10, S11, ESI†). In the presence of both MMP and NIR, all cells were killed by the introduction of Au@SiO_2/DOX@Pep nanocapsules and showed typical red fluorescence.

In vivo experiments involving gold-silica nanocapsules using a tumor-xenografted mouse model were also carried out. As visualized using a photothermal camera, the local temperature of the irradiated tumor region increased to 55 °C within 10 minutes upon NIR exposure at 1.0 W cm^{-2} (Fig. 4a). The hyperthermal effect was concluded to be sufficient for the photothermal treatments. Consistent with the *in vitro* experiments, the tumor-bearing mice in Au@SiO_2/DOX@Pep + NIR group achieved the best antitumor efficacy (Fig. 4b and Fig. S13, ESI†). All mice under chemo-photothermal combination treatment survived, and their tumors had been entirely ablated within 14 days (Fig. 4c). Parallel experiments with other mice cohorts showed much lower antitumor efficiency either in the absence of drug loading or NIR irradiation. Corresponding H&E staining verified the effectiveness of the chemo-photothermal combination treatment, as substantial tissue necrosis was observed in sampled tumor section profiles (Fig. 4d). During the period of treatment, mice dosed with Au@SiO_2/DOX@Pep and NIR irradiation showed no significant changes in body weight (Fig. S14, ESI†). Histological analysis indicated that use of Au@SiO_2/DOX@Pep would not induce tissue damage or inflammatory lesion to major organs (heart, liver, spleen, lung, and kidney in Fig. S15, ESI†). All above assessments collectively implied that the peptide-photowrapped gold-silica platform could encapsulate a therapeutic drug, respond to the tumor microenvironment, and realize photomanipulated combination therapy with favorable anticancer efficacy.

In conclusion, we designed and synthesized a multifunctional undecapeptide, YYDPLGLADYY, for the fabrication of gold-silica nanocapsules by means of photochemistry. Utilizing a photocrosslinking strategy involving YY motifs, surface-modified Au@SiO_2 could be photowrapped with peptide and form a well-defined core–shell structure. The obtained gold-silica nanocapsules are able to

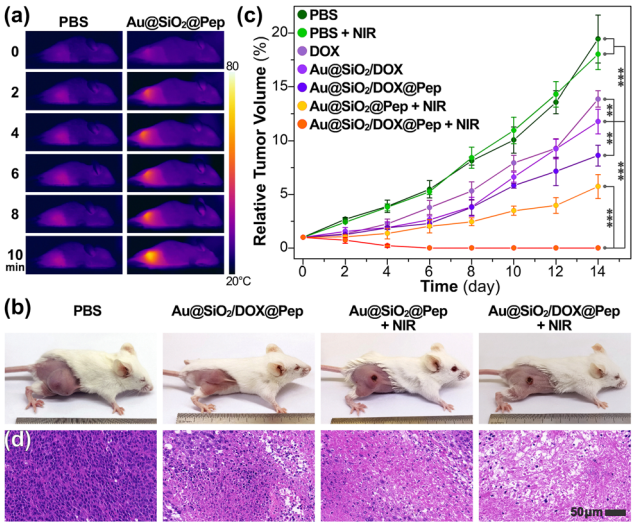

Fig. 4 (a) *In vivo* thermal images of tumor-bearing mice treated with PBS and Au@SiO_2@ Pep under NIR irradiation recorded at indicated time intervals. (b) Photographs of tumor-bearing mice at day 14 after being subjected to indicated treatments (n = 5). (c) Relative tumor volume and (d) H&E staining of tumor sections in indicated groups. **, $p < 0.01$; ***, $p < 0.001$.

encapsulate DOX as a model drug and respond to an MMP-upregulated tumor microenvironment through the PLGLA segment of the peptide. More importantly, an NIR stimulus could be applied as a remote manipulation pathway to realize anticancer chemo-photothermal therapy with favorable efficacy.

This work was financially supported by the Beijing Natural Science Foundation (2222051) and the National Natural Science Foundation of China (81973442). The authors also acknowledge the technical support provided by the Core Facility Center at CCMU.

Conflicts of interest

There are no conflicts to declare.

Notes and references

1 J. Shi, P. W. Kantoff, R. Wooster and O. C. Farokhzad, *Nat. Rev. Cancer*, 2017, **17**, 20–37.
2 M. T. Manzari, Y. Shamay, H. Kiguchi, N. Rosen, M. Scaltriti and D. A. Heller, *Nat. Rev. Mater.*, 2021, **6**, 351–370.
3 R. Kumari, D. Sunil and R. S. Ningthoujam, *J. Controlled Release*, 2020, **319**, 135–156.
4 Y. Li, K. Tang, X. Zhang, W. Pan, N. Li and B. Tang, *Chem. Commun.*, 2022, **58**, 8754–8765.
5 M. De Palma, D. Biziato and T. V. Petrova, *Nat. Rev. Cancer*, 2017, **17**, 457–474.
6 J. Vandooren, G. Opdenakker, P. M. Loadman and D. R. Edwards, *Adv. Drug Delivery Rev.*, 2016, **97**, 144–155.
7 Y. Lu, A. A. Aimetti, R. Langer and Z. Gu, *Nat. Rev. Mater.*, 2016, **2**, 16075.
8 Q. Jin, Y. Deng, X. Chen and J. Ji, *ACS Nano*, 2019, **13**, 954–977.
9 K. Li, C.-J. Liu and X.-Z. Zhang, *Adv. Drug Delivery Rev.*, 2020, **160**, 36–51.
10 X. Dong, R. K. Brahma, C. Fang and S. Q. Yao, *Chem. Sci.*, 2022, **13**, 4239–4269.
11 N.-Y. Zhang, X.-J. Hu, H.-W. An, J.-X. Liang and H. Wang, *Biomaterials*, 2022, **287**, 121655.
12 X. Li, A. n Sun, Y.-j Liu, W.-j Zhang, N. Pang, S.-x Cheng and X.-r Qi, *NPG Asia Mater.*, 2018, **10**, 238–254.
13 Z. Fan, C. Jiang, Y. Wang, K. Wang, J. Marsh, D. Zhang, X. Chen and L. Nie, *Nanoscale Horiz.*, 2022, **7**, 682–714.
14 Z. Ge and S. Liu, *Chem. Soc. Rev.*, 2013, **42**, 7289–7325.
15 J. Pan, P.-J. Li, Y. Wang, L. Chang, D. Wan and H. Wang, *Chem. Commun.*, 2018, **54**, 11092–11095.
16 H. Wang, L. Gao, T. Fan, C. Zhang, B. Zhang, O. A. Al-Hartomy, A. Al-Ghamdi, S. Wageh, M. Qiu and H. Zhang, *ACS Appl. Mater. Interfaces*, 2021, **13**, 54621–54647.
17 Y. Li, X. Zhang, Z. Zhang, H. Wu, X. Xu and Z. Gu, *Mater. Horiz.*, 2018, **5**, 1047–1057.
18 T. Liang, B. Zhang, Z. Xing, Y. Dong, H. Xu, X. Chen, L. Jiang, J.-J. Zhu and Q. Min, *Angew. Chem., Int. Ed.*, 2021, **60**, 11464–11473.
19 H. S. El-Sawy, A. M. Al-Abd, T. A. Ahmed, K. M. El-Say and V. P. Torchilin, *ACS Nano*, 2018, **12**, 10636–10664.
20 M. Wang, B. Gao, X. Wang, W. Li and Y. Feng, *Biomater. Sci.*, 2022, **10**, 1883–1903.
21 J. Wang, J. Liu, Y. Liu, L. Wang, M. Cao, Y. Ji, X. Wu, Y. Xu, B. Bai, Q. Miao, C. Chen and Y. Zhao, *Adv. Mater.*, 2016, **28**, 8950–8958.
22 H. P. Tham, H. Chen, Y. H. Tan, Q. Qu, S. Sreejith, L. Zhao, S. S. Venkatraman and Y. Zhao, *Chem. Commun.*, 2016, **52**, 8854–8857.
23 Q. Chen, Z. Li, J. Yu, Q. Xie, H. Lu, Y. Deng, J. Chen, W. Zhu, L. Huo, Y. Zhang, W. Song, J. Lan, J. Cai, Z. Huang, Z. Wang and H. Zhao, *Nano Res.*, 2022, **15**, 9149–9159.
24 A. Liu, G. Wang, F. Wang and Y. Zhang, *Coord. Chem. Rev.*, 2017, **336**, 28–42.
25 Y. Wu, F. Chen, N. Huang, J. Li, C. Wu, B. Tan, Y. Liu, L. Li, C. Yang, D. Shao and J. Liao, *Nanoscale*, 2021, **13**, 17168–17182.
26 B. Yang and J. Shi, *Acc. Mater. Res.*, 2021, **2**, 581–593.
27 W. Chen, C. A. Glackin, M. A. Horwitz and J. I. Zink, *Acc. Chem. Res.*, 2019, **52**, 1531–1542.
28 J. Wen, K. Yang, F. Liu, H. Li, Y. Xu and S. Sun, *Chem. Soc. Rev.*, 2017, **46**, 6024–6045.
29 C. Li, K. Feng, N. Xie, W. Zhao, L. Ye, B. Chen, C.-H. Tung and L.-Z. Wu, *ACS Appl. Nano Mater.*, 2020, **3**, 5070–5078.
30 J. Zhao, C. Li, X.-W. Gao, K. Feng, H. Liu, S. He, W. Zhao, S. Yang, J. Shao, L. Ye, B. Chen, N. Xie, C.-H. Tung and L.-Z. Wu, *Nano Res.*, 2023, **16**, 4029–4038.
31 N.-Q. Shi and X.-R. Qi, *ACS Appl. Mater. Interfaces*, 2017, **9**, 10519–10529.
32 B. Tan, Y. Wu, Y. Wu, K. Shi, R. Han, Y. Li, Z. Qian and J. Liao, *ACS Appl. Mater. Interfaces*, 2021, **13**, 31542–31553.
33 Y. Li, D. Hu, M. Pan, Y. Qu, B. Chu, J. Liao, X. Zhou, Q. Liu, S. Cheng, Y. Chen, Q. Wei and Z. Qian, *Biomaterials*, 2022, **288**, 121700.

